MSDE

PAPER

View Article Online
View Journal | View Issue

Cite this: *Mol. Syst. Des. Eng.*, 2025, **10**, 184

Nanostructured liquid-crystalline ion conductors based on linear carbonate moieties: effects of oligooxyethylene and alkylene spacers on self-assembled properties and ionic conductivities†

Junya Uchida, [a] Shingo Takegawa, [a] Soshi Ito, [a] Shunsuke Sato, [b] Go Watanabe [bcd] and Takashi Kato *[ae]

Received 29th October 2024,
Accepted 4th January 2025

DOI: 10.1039/d4me00176a

rsc.li/molecular-engineering

We here report rodlike liquid-crystalline (LC) molecules consisting of bicyclohexyl and linear carbonate moieties connected through flexible spacers for the development of nanostructured ion-conductive materials. The molecular assemblies of the linear carbonate-based rodlike compounds mixed with a lithium salt provide 2D ion-conductive pathways in the smectic LC phases. The LC materials containing polar oligooxyethylene spacers coupled with linear carbonate moieties have been shown to function as efficient ion conductors, while those containing nonpolar alkylene spacers form thermally stable and ordered smectic LC structures. Molecular dynamics simulations provide insights into the conformation and packing of the molecules containing oligooxyethylene spacers in the LC phases. The combination of flexible oligooxyethylene chains and linear carbonates may lead to design of new LC electrolytes with highly mobile 2D nanochannels for applications in energy devices.

Design, System, Application

Self-assembly of liquid-crystalline (LC) molecules has attracted attention for the development of dynamic and ordered functional materials in a variety of fields of energy and environmental sciences. Herein, molecular engineering of new LC ion conductors containing linear carbonate moieties is demonstrated by experimental and computational approaches. Transport materials with 2D ion-conductive pathways are obtained by self-assembly of the linear carbonate-based smectic liquid crystals complexed with a lithium salt. These materials have potential as quasi-solid-state self-assembled electrolytes in energy devices. We previously used cyclic carbonate-based ion-conductive 2D nanostructured liquid crystals for electrolytes in lithium-ion batteries. The present design based on linear carbonate moieties may lead to preparation of LC electrolytes forming highly mobile 2D nanochannels for applications in lithium-ion batteries.

Introduction

Nanostructured liquid crystals have attracted much attention towards the development of dynamic and anisotropic functional materials.[1–13] In particular, use of ordered nanostructures of liquid crystals allows efficient transport of ions,[14–22] electrons,[14,23–26] and water molecules,[13,27–32] leading to the preparation of energy devices and water treatment membranes. Lithium-ion conductive nanostructured liquid crystals are one of the candidates for application as electrolytes in lithium-ion batteries because of their self-assembled ion-transport pathways and nonvolatility.[6,14,15,33–41] The transport of lithium ions in 1D,[42–46] 2D,[47–62] and 3D[42,46,63–67] nanostructures has been reported for columnar, smectic, and bicontinuous liquid-crystalline (LC) materials, respectively.

Our intention here is to develop 2D lithium-ion conductive LC materials based on linear carbonate moieties combined with oligooxyethylene chains (Fig. 1). We have developed cyclic carbonate-based smectic liquid crystals forming 2D ion-transport nanochannels and applied as electrolytes in lithium-ion batteries.[33–36] High oxidation resistance was achieved for a

[a] *Department of Chemistry and Biotechnology, School of Engineering, The University of Tokyo, Hongo, Bunkyo-ku, Tokyo 113-8656, Japan. E-mail: kato@chiral.t.u-tokyo.ac.jp*
[b] *Department of Physics, School of Science, Kitasato University, Sagamihara, Kanagawa 252-0373, Japan*
[c] *Department of Data Science, School of Frontier Engineering, Kitasato University, Sagamihara, Kanagawa 252-0373, Japan*
[d] *Kanagawa Institute of Industrial Science and Technology (KISTEC), Ebina, Kanagawa 242-0435, Japan*
[e] *Institute for Aqua Regeneration, Shinshu University, Wakasato, Nagano 380-8553, Japan*

† Electronic supplementary information (ESI) available. See DOI: https://doi.org/10.1039/d4me00176a

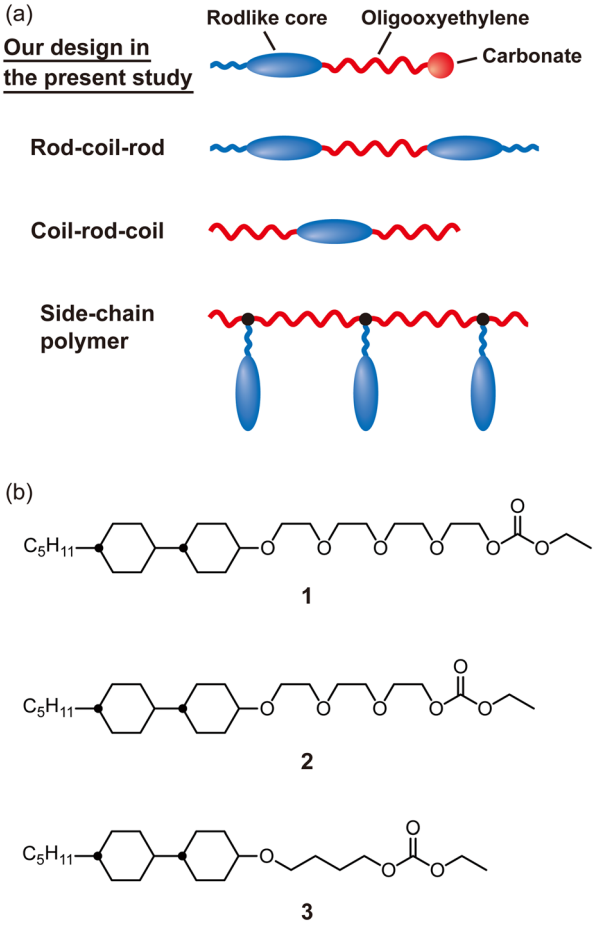

Fig. 1 (a) Schematic illustration of molecular design of lithium-ion conductive smectic liquid crystals containing oligooxyethylene chains. (b) Molecular structures of compounds **1**–**3**.

cyclic carbonate-based smectic LC electrolyte containing an electrochemically stable bicyclohexyl moiety and a flexible oligooxyethylene spacer.[35] While cyclic carbonates have higher dielectric constants to dissociate lithium salts, linear carbonates have lower viscosity to promote ion transport.[68,69] We expected that combination of linear carbonates, oligooxyethylene chains, and bicyclohexyl moieties would provide new nanostructured LC materials forming 2D ion-conductive pathways with higher fluidity.

Self-assembly of precisely designed molecules has led to the formation of a variety of 2D nanoscale assemblies.[70,71] Introduction of functional moieties into rodlike molecules has been an approach to provide functional smectic LC materials.[72–87] In the design of 2D lithium-ion conductive liquid crystals, polar ion-conductive moieties such as carbonates[33–36,52,55,58,62] and oligooxyethylene chains[35,47–56,62] as well as ionic moieties[40,59–61] were attached to nonpolar rodlike molecules to form self-assembled nanochannels in the smectic LC phases through nanosegregation.

Here we report design and synthesis of ion-conductive liquid crystals **1**–**3** consisting of bicyclohexyl and linear carbonate moieties connected through flexible spacers (Fig. 1b). Self-assembled properties and ionic conductivities of these linear carbonate-based LC materials containing oligooxyethylene and alkylene spacers were studied. In addition, molecular conformation and packing of the compounds containing oligooxyethylene spacers in the LC phases were examined by molecular dynamics (MD) simulations.

Results and discussion

Molecular design

Compounds **1**–**3** are composed of bicyclohexyl cores, flexible spacers, and linear carbonate moieties. These rodlike molecules are intended to form smectic LC phases through nanosegregation between polar and nonpolar moieties. We previously reported electrochemically stable LC electrolytes, where a cyclic carbonate and a bicyclohexyl core were linked through an oligooxyethylene spacer.[35] In the present study, the linear carbonate moieties coupled with oligooxyethylene spacers for compounds **1** and **2** are expected to provide more mobile 2D nanochannels in the LC phases as well as to dissolve lithium salts. Compound **3** having an alkylene spacer was designed to study the effects of flexible spacers binding bicyclohexyl and linear carbonate moieties on the self-assembled properties and ionic conductivities of these LC mixtures with a lithium salt.

Liquid-crystalline properties of compounds 1–3

LC properties of compounds **1**–**3** were examined by polarizing optical microscopy (POM), differential scanning calorimetry (DSC), and X-ray diffraction (XRD) measurements (Table 1, Fig. 2, S1 and S2†). Compounds **1** and **2** bearing oligooxyethylene spacers exhibited smectic B phases with similar clearing temperatures. Compound **3** bearing an alkylene spacer showed a more ordered and thermally stable smectic phase than those of compounds **1** and **2**. The flexible oligooxyethylene chains may lower the phase transition temperatures of **1** and **2**.

Compounds **1**–**3** exhibited optical textures under POM observations in the LC phases at 30 °C (Fig. 2, left and S2†), which are characteristic of the formation of smectic phases. The XRD pattern of **1** at 30 °C gives periodic peaks at 31.8, 15.7, and 10.4 Å with a small peak at 4.9 Å (Fig. 2a, right). Similar XRD pattern is observed for compound **2** in the LC phase (Fig. 2b, right). These results show that compounds **1** and **2** exhibited smectic B phases. The average layer spacings

Table 1 Phase transition behavior of compounds **1**–**3**

Compound	Phase transition behavior[a,b]		
1	SmB	44 (7)	Iso
2	SmB	47 (7)	Iso
3	Sm	71 (7)	Iso

[a] Transition temperatures (°C) and enthalpies (kJ mol^{-1}, given in parentheses) were determined by differential scanning calorimetry (DSC) on the second heating at the scanning rate of 10 °C min^{-1}. [b] Iso: isotropic; SmB: smectic B; Sm: unidentified smectic.

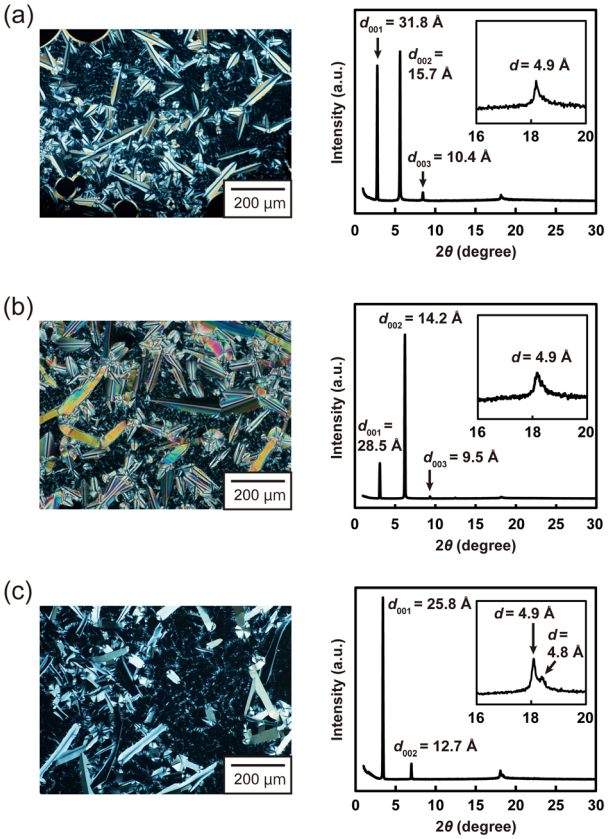

Fig. 2 Polarizing optical micrographs (left panels) and XRD patterns (right panels): (a) compound **1** in the smectic B phase at 30 °C, (b) compound **2** in the smectic B phase at 30 °C, and (c) compound **3** in the smectic phase at 30 °C.

for **1** and **2** were estimated to be 32 and 28 Å, respectively. They are smaller than the extended molecular lengths estimated with molecular modelling (35 Å for **1** and 31 Å for **2**) (Fig. S3†) probably because the flexible oligooxyethylene chains were not fully extended in the LC states.[62] For compound **3**, the formation of a highly ordered smectic LC phase was proposed because two peaks in the wide-angle region as well as periodic peaks corresponding to a layered structure were observed (Fig. 2c, right). The average layer spacing for **3** was estimated to be 26 Å, which is the same as the extended molecular length of **3** (Fig. S3†). These results suggest that compounds **1**–**3** formed monolayer structures in the smectic LC phases.

Addition of a lithium salt to compounds 1–3

Phase transition properties of the mixtures of compounds **1**–**3** and lithium bis(trifluoromethylsulfonyl)imide (LiTFSI) were examined (Table 2 and Fig. S4–S15†). Complexes of **1** and LiTFSI (**1**/LiTFSI) and **2**/LiTFSI exhibited only smectic B phases at lower concentrations of LiTFSI, while they formed smectic A phases at higher concentrations of LiTFSI. Similar phase transitions from smectic B to smectic A phases by the introduction of LiTFSI were reported for cyclic carbonate-based

Table 2 Phase transition behavior of the mixtures of the LC molecules and LiTFSI

Mixture	Phase transition behavior[a,b]				
1/LiTFSI (9 : 1)	SmB	42	Iso		
1/LiTFSI (8 : 2)	SmB	44	Iso		
1/LiTFSI (7 : 3)	SmB	46	Iso		
1/LiTFSI (6 : 4)	SmA	43	Iso		
2/LiTFSI (9 : 1)	SmB	44	Iso		
2/LiTFSI (8 : 2)	SmB	42	Iso		
2/LiTFSI (7 : 3)	SmB	42	SmA	51	Iso
2/LiTFSI (6 : 4)	SmB	23	SmA	45	Iso
3/LiTFSI (9 : 1)	Sm	74	Iso		
3/LiTFSI (8 : 2)	Sm	82	Iso		
3/LiTFSI (7 : 3)	Sm	81	Iso		
3/LiTFSI (6 : 4)	Sm	86	Iso		

[a] Transition temperatures (°C) were determined by differential scanning calorimetry (DSC) on the second heating at the scanning rate of 10 °C min^{-1}. [b] Iso: isotropic; SmA: smectic A; SmB: smectic B; Sm: unidentified smectic.

liquid crystals bearing oligooxyethylene chains.[35] The clearing temperatures of **1**/LiTFSI and **2**/LiTFSI were the highest for the mixtures in the molar ratios of 7 : 3 (Table 2). The effects of the addition of LiTFSI on the clearing temperatures were not significant. The clearing temperatures of **3**/LiTFSI showed an increasing trend with increasing the concentration of LiTFSI (Table 2). This increase in the clearing temperatures of **3**/LiTFSI may be due to stabilization of the LC phases through ion–dipole interactions between the lithium ion and the linear carbonate moiety of **3**.[33,34] For **1**/LiTFSI and **2**/LiTFSI, the stabilization of the LC phases through the interactions between the lithium ion and the linear carbonate moieties may be weakened by the interactions between the lithium ion and oligooxyethylene chains.[52]

The interactions between the linear carbonate moieties of **1**–**3** and LiTFSI were studied by Fourier transform infrared (FT-IR) spectroscopy (Fig. 3 and S16†). The absorption peaks corresponding to C=O stretching vibrations of the linear carbonates for **1**–**3** appear at 1747 cm^{-1}. The lower wavenumber shifts of these peaks are observed by addition of LiTFSI to compounds **1**–**3** (Fig. 3 and S16†), indicating that the linear carbonate moieties of **1**–**3** interacted with the lithium ion. It should be noted that the spacers binding bicyclohexyl cores and linear carbonates affected the interactions between the linear carbonate moieties and the lithium ion. The peaks at 1747 cm^{-1} are clearly observed for **1**/LiTFSI (6 : 4) and **2**/LiTFSI (6 : 4) (Fig. 3a and S16†), while the peak almost disappears for **3**/LiTFSI (6 : 4) (Fig. 3b). These results show that the ratio of linear carbonates interacting with the lithium ion was lower for oligooxyethylene-based compounds **1** and **2** than that for alkylene-based compound **3**. The oligooxyethylene chains as well as terminal linear carbonates of **1** and **2** may incorporate the lithium ion in the smectic LC assemblies.[35,47–56,62]

The effects of addition of LiTFSI to the smectic LC assemblies of **1**–**3** on the layer spacings were examined (Fig. 4). The layer spacings of **1**/LiTFSI and **2**/LiTFSI in the smectic B

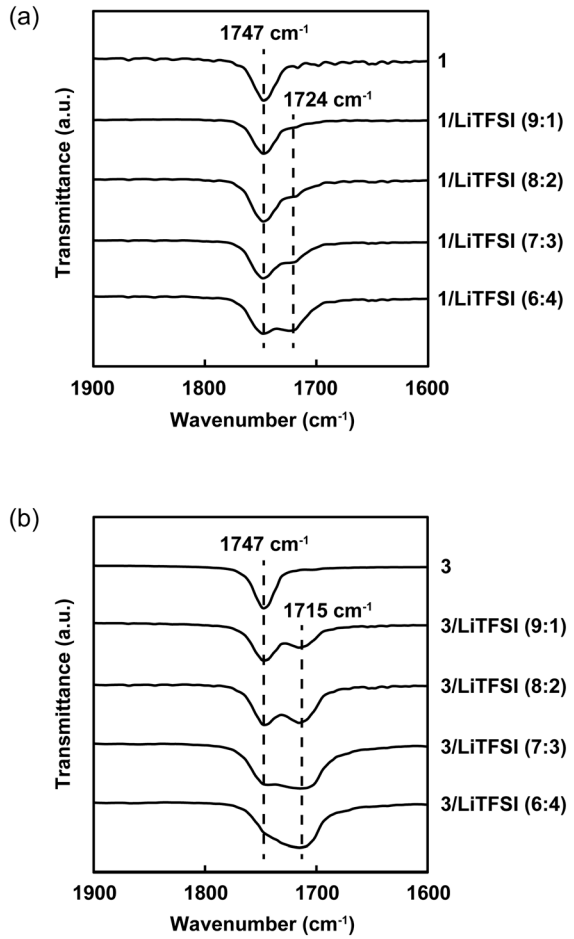

Fig. 3 FT-IR spectra of the LC mixtures with different molar ratios of LiTFSI: (a) **1**/LiTFSI at 30 °C and (b) **3**/LiTFSI at 30 °C.

phases increased with increasing the concentration of LiTFSI up to 30 mol%. The incorporation of LiTFSI into the 2D nanostructures in the smectic LC phases may affect the interdigitation of polar moieties of **1** and **2**. For **1**/LiTFSI (6 : 4) and **2**/LiTFSI (6 : 4) in the smectic A phases, the layer spacings were almost identical to those for **1**/LiTFSI (7 : 3) and **2**/LiTFSI (7 : 3) in the smectic B phases, respectively (Fig. 4). These results suggest that the loss of hexatic order of the smectic B phases changed the molecular packing and conformation of compounds **1** and **2** having the oligooxyethylene spacers.[62] For **3**/LiTFSI forming highly ordered smectic phases, the layer spacing increased with increasing the concentration of LiTFSI up to 40 mol% (Fig. 4).

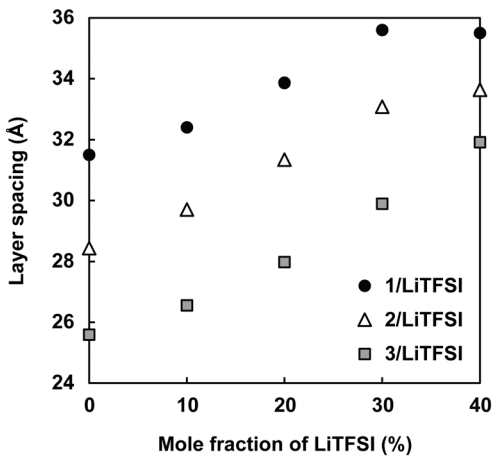

Fig. 4 Layer spacings of **1**/LiTFSI, **2**/LiTFSI, and **3**/LiTFSI in the smectic LC phases at 30 °C.

Based on the XRD measurements and FT-IR spectroscopy, possible self-assembled structures of the LC mixtures are shown in Fig. 5. It is proposed that nanosegregation between bicyclohexyl cores and linear carbonate moieties linked with oligooxyethylene spacers provides 2D ion-conductive layers for **1**/LiTFSI and **2**/LiTFSI (Fig. 5a). The polar ion-conductive layers are considered to incorporate LiTFSI in the smectic LC phases. For **3**/LiTFSI, 2D ion-conductive layers are proposed to be formed by self-assembly of the linear carbonate moiety complexed with LiTFSI (Fig. 5b). The polarity of the spacers binding linear carbonate moieties and bicyclohexyl cores may affect complexation of the LC molecules with LiTFSI and formation of the 2D nanostructured ion-conductive pathways.

Ionic conductivities

The ionic conductivities of the LC mixtures of **1**/LiTFSI, **2**/LiTFSI, and **3**/LiTFSI were measured by an alternating current

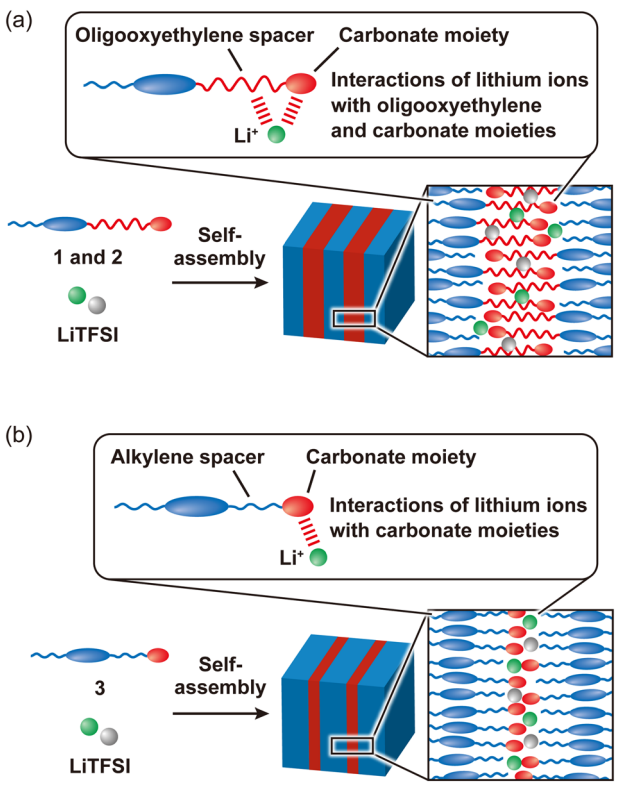

Fig. 5 Schematic illustration of possible self-assembled structures of the LC mixtures: (a) **1**/LiTFSI and **2**/LiTFSI having oligooxyethylene spacers and (b) **3**/LiTFSI having alkylene spacers.

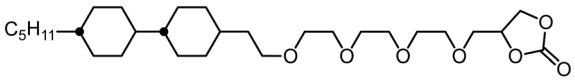

4

Fig. 6 Molecular structure of cyclic carbonate-based LC compound **4**.

impedance method using comb-shaped gold electrodes deposited on a glass substrate. The effects of the concentration of LiTFSI on the ionic conductivities were examined for the LC mixtures (Fig. S17–S19†). LC mixtures **1**/LiTFSI (7 : 3), **2**/LiTFSI (8 : 2), and **3**/LiTFSI (8 : 2) exhibited the highest ionic conductivities at 30 °C among the mixtures based on compounds **1**, **2**, and **3**, respectively (Fig. S17–S19†). Generally, higher ionic conductivities are obtained for electrolytes with higher number of ions and lower viscosity.[68] The balance of these two parameters was optimal when the concentration of LiTFSI was 20 mol% for **2**/LiTFSI and **3**/LiTFSI. For **1**/LiTFSI, the longer flexible oligooxyethylene chain may suppress the increase of the viscosity at higher concentration of LiTFSI. The highest ionic conductivities were achieved when the concentration of LiTFSI was 30 mol% for **1**/LiTFSI. LC mixtures **1**/LiTFSI (7 : 3), **2**/LiTFSI (8 : 2), and **3**/LiTFSI (8 : 2) were selected as representative materials for the following discussion on the ionic conductivities. The ionic conductivities of these LC mixtures were compared with those of cyclic carbonate-based LC compound **4** (ref. 35) (Fig. 6) mixed with LiTFSI (Fig. 7). The mixtures of compound **4** and LiTFSI were previously used as LC electrolytes with high oxidation resistance in lithium-ion batteries.[35] The ionic conductivities of **1**/LiTFSI (7 : 3) and **2**/LiTFSI (8 : 2) in the smectic B phases at 30 °C were 1.0×10^{-5} and 9.1×10^{-6} S cm^{-1}, respectively (Fig. 7). These values were higher than those of **4**/LiTFSI (8 : 2) at 30 °C (5.3×10^{-6} S cm^{-1}) (Fig. 7). The mobile 2D ion-conductive pathways formed from linear carbonate moieties and flexible oligooxyethylene chains (Fig. 5a) may lead to efficient ion transport for **1**/LiTFSI and **2**/LiTFSI in the LC phases. For **3**/LiTFSI (8 : 2) having alkylene spacers, the ionic conductivities were lower than those of **1**/LiTFSI (7 : 3), **2**/LiTFSI (8 : 2), and **4**/LiTFSI (8 : 2) probably due to the less mobile structures in the LC phase (Fig. 5b).

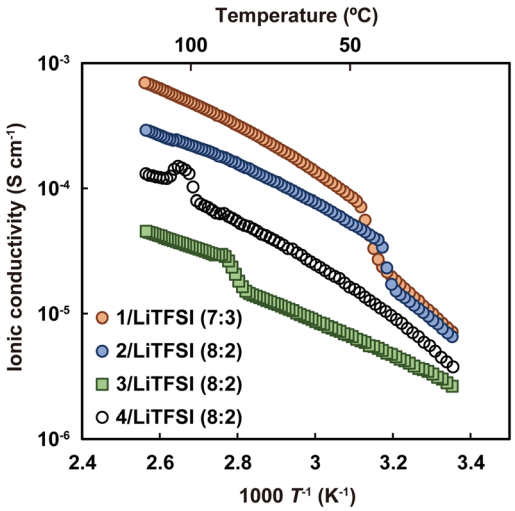

Fig. 7 Ionic conductivities of **1**/LiTFSI (7 : 3), **2**/LiTFSI (8 : 2), **3**/LiTFSI (8 : 2), and **4**/LiTFSI (8 : 2).

Molecular dynamics simulations

To understand the details of the molecular alignment of compounds **1** and **2** in the smectic B phases, MD simulations were performed (Fig. 8 and S20–S23†). The MD simulations

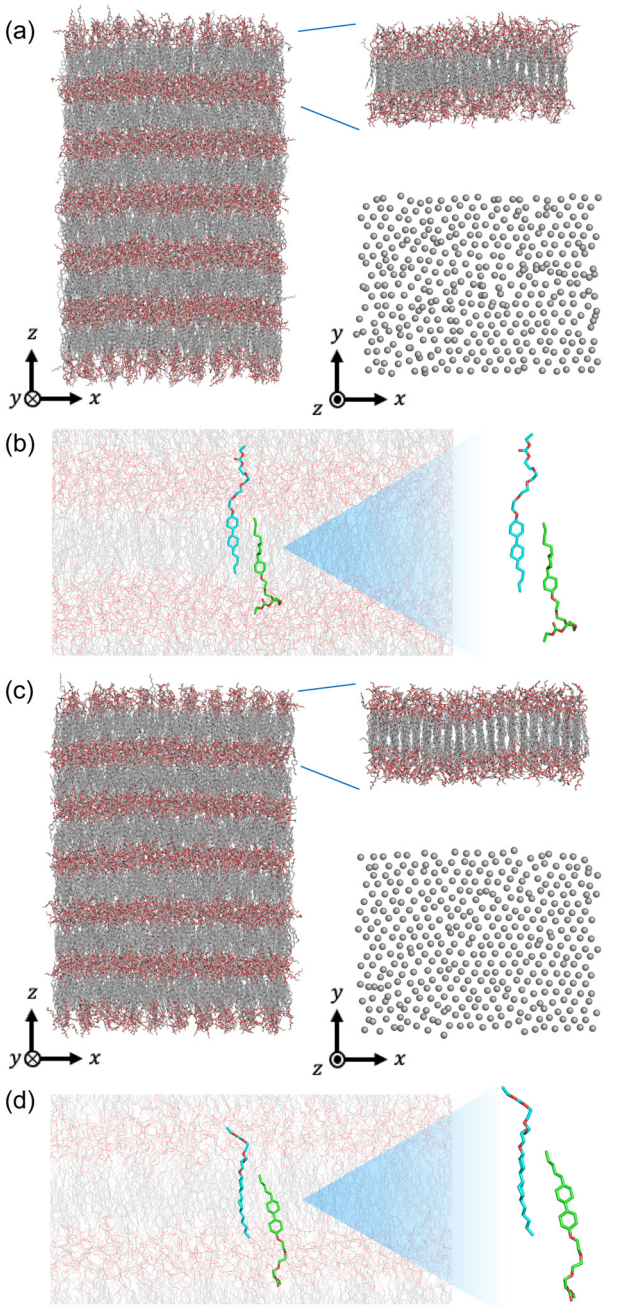

Fig. 8 Side views of MD simulation snapshots and top views of the centers of the mass of the molecules: (a) compound **1** and (c) compound **2**. Partially enlarged snapshots: (b) compound **1** and (d) compound **2**.

show that compounds **1** and **2** formed the smectic layers of which the average layer spacings are 3.04 nm and 2.81 nm, respectively (Fig. 8). These values were close to those obtained by the XRD measurements (Fig. 2a, right and b, right). From the top view snapshots of the center of the mass of the molecules, it can be found that the molecules mostly aligned to maintain the hexatic symmetry in the layers (Fig. 8a and c). In the layers of both systems of compounds **1** and **2**, the bicyclohexyl cores and terminal alkyl chains of the molecules showed averagely interdigitated alignment parallel to the layer normal at 30 °C (Fig. 8b and d). In addition, the order parameters determined by the MD simulations show that the bicyclohexyl cores were highly oriented compared to the oligooxyethylene chains (Fig. S22 and S23†). For both systems of compounds **1** and **2**, the order parameters of bicyclohexyl cores were 0.8–0.9, while those of oligooxyethylene chains were 0.4–0.6 (Fig. S22 and S23†). These results support the formation of the mobile 2D nanochannels by self-assembly of **1** and **2** in the smectic LC phases.

Conclusions

A series of linear carbonate-based 2D ion-conductive liquid crystals has been designed and synthesized. These molecules and their mixtures with LiTFSI exhibit smectic LC phases. We have demonstrated that the spacers binding bicyclohexyl cores and linear carbonate moieties significantly affect the self-assembled properties and ionic conductivities of these materials. The mixtures of LC molecules containing oligooxyethylene spacers and LiTFSI exhibit higher ionic conductivities than the mixtures of LC molecules containing alkylene spacers and LiTFSI. The combination of flexible oligooxyethylene chains and linear carbonates may be useful to design highly mobile 2D nanochannels for transport of ions. These LC materials have potential for use as components of electrolytes in energy devices including lithium-ion batteries.

Experimental section

General procedures

^{1}H and ^{13}C nuclear magnetic resonance (NMR) spectra were recorded on a JEOL JNM-ECX400 spectrometer at 400 and 100 MHz, respectively. The chemical shifts of the ^{1}H and ^{13}C NMR signals were referenced to the $Si(CH_3)_4$ (δ = 0.00) and $CDCl_3$ (δ = 77.00) as internal standards, respectively. Matrix-assisted laser desorption ionization time-of-flight mass spectrometry (MALDI-TOF-MS) was conducted with a Bruker autoflex speed spectrometer using dithranol as the matrix. Elemental analyses were performed on an Exeter Analytical CE440 elemental analyzer. Fourier transform infrared (FT-IR) spectroscopy was carried out with a JASCO FT/IR-6100 Plus spectrometer and a JASCO IRT-5000 spectrometer with a Linkam 10084L hot stage. Polarizing optical micrographs were taken with an Olympus BX51 microscope equipped with a Linkam 10084L hot stage. Differential scanning calorimetry (DSC) was conducted using NETZSCH DSC 3500 Sirius with a scanning rate of 10 °C min^{-1}. X-ray diffraction (XRD) patterns were obtained with a Rigaku RINT-2500 diffractometer using Ni-filtered CuKα radiation.

Materials

All reagents and solvents for the synthesis of the LC molecules were purchased from Tokyo Chemical Industry (Tokyo, Japan), FUJIFILM Wako Pure Chemical (Osaka, Japan), Sigma-Aldrich Japan (Tokyo, Japan), and Kanto Chemical (Tokyo, Japan). Lithium bis(trifluoromethylsulfonyl)imide (LiTFSI) was obtained from Kishida Chemical (Osaka, Japan). They were used as received. Unless otherwise noted, the reactions were performed under an argon atmosphere in dry solvents. 2-(2-(2-(2-((Tetrahydro-2*H*-pyran-2-yl)oxy)ethoxy)ethoxy)ethoxy)ethyl 4-methylbenzenesulfonate,[88] 2-(2-(2-((tetrahydro-2*H*-pyran-2-yl)oxy)ethoxy)ethoxy)ethyl 4-methylbenzenesulfonate,[89] and 2-(4-bromobutoxy)tetrahydro-2*H*-pyran[90] were synthesized as reported.

Synthesis of LC molecules 1–3

Synthesis of 2-(2-(2-(2-((*trans*,*trans*-4′-pentyl-[1,1′-bi(cyclohexan)]-4-yl)oxy)ethoxy)ethoxy)ethoxy)ethan-1-ol. To a stirred mixture of 18-crown-6 (0.573 g, 2.17 mmol), *trans*, *trans*-4′-pentyl-[1,1′-bi(cyclohexan)]-4-ol (0.540 g, 2.14 mmol), and 2-(2-(2-(2-((tetrahydro-2*H*-pyran-2-yl)oxy)ethoxy)ethoxy)ethoxy)ethyl 4-methylbenzenesulfonate (1.02 g, 2.35 mmol) in tetrahydrofuran (THF) (5 mL), potassium *tert*-butoxide (0.368 g, 3.28 mmol) was slowly added at 0 °C. The mixture was stirred at 25 °C for 70 h. After slowly adding water to the solution, the mixture was extracted with chloroform. The organic layer was washed with brine and dried over anhydrous $MgSO_4$, filtered, and evaporated under reduced pressure. To the residue dissolved in ethanol (25 mL) and THF (10 mL) was added 5% hydrochloric acid (8 mL) and the solution was stirred at 25 °C for 8 h. The mixture was extracted with chloroform. The organic layer was washed with brine and dried over anhydrous $MgSO_4$. After filtration and evaporation of the solvent, the crude product was purified by silica gel column chromatography (eluent: hexane/ethyl acetate = 35 : 65 to 25 : 75 (v/v)) to give the product (0.390 g, 43% yield). ^{1}H NMR (400 MHz, $CDCl_3$): δ = 3.75–3.59 (m, 16H), 3.22–3.13 (m, 1H), 3.03 (brs, 1H), 2.09–2.01 (m, 2H), 1.78–1.65 (m, 6H), 1.33–0.77 (m, 22H). ^{13}C NMR (100 MHz, $CDCl_3$): δ = 79.1, 72.6, 70.9, 70.6, 70.5, 70.2, 67.2, 61.7, 42.9, 42.5, 37.8, 37.4, 33.6, 32.4, 32.2, 30.2, 28.1, 26.6, 22.7, 14.1. MS (MALDI-TOF): calcd. (m/z) for $[M + Na]^+$, 451.34; found, 451.12.

Synthesis of compound 1. A mixture of 2-(2-(2-(2-((*trans*, *trans*-4′-pentyl-[1,1′-bi(cyclohexan)]-4-yl)oxy)ethoxy)ethoxy)ethoxy) ethan-1-ol (0.305 g, 0.711 mmol) and KF/Al_2O_3 (0.150 g) in diethyl carbonate (15 mL) was refluxed for 6 h. The reaction mixture was diluted with CH_2Cl_2 and filtered to remove KF/

Al_2O_3. After evaporation of the solvent, the crude product was purified by silica gel column chromatography (eluent: hexane/ethyl acetate = 1 : 1 (v/v)) to give compound **1** (0.322 g, 92% yield). ^{1}H NMR (400 MHz, $CDCl_3$): δ = 4.30–4.26 (m, 2H), 4.20 (q, J = 7.2 Hz, 2H), 3.74–3.71 (m, 2H), 3.67–3.61 (m, 12H), 3.21–3.12 (m, 1H), 2.09–2.00 (m, 2H), 1.79–1.65 (m, 6H), 1.35–0.77 (m, 25H). ^{13}C NMR (100 MHz, $CDCl_3$): δ = 155.1, 79.0, 70.9, 70.6, 70.6, 68.9, 67.2, 66.8, 64.0, 42.9, 42.6, 37.8, 37.4, 33.6, 32.5, 32.2, 30.2, 28.1, 26.6, 22.7, 14.2, 14.1. MS (MALDI-TOF): calcd. (m/z) for $[M + Na]^+$, 523.36; found, 523.18. Elemental analysis: calcd. (%) for $C_{28}H_{52}O_7$: C 67.17, H 10.47; found: C 67.09, H 10.74.

Synthesis of 2-(2-(2-((*trans*,*trans*-4′-pentyl-[1,1′-bi(cyclohexan)]-4-yl)oxy)ethoxy)ethoxy)ethan-1-ol. To a stirred mixture of 18-crown-6 (1.057 g, 4.00 mmol), *trans*,*trans*-4′-pentyl-[1,1′-bi(cyclohexan)]-4-ol (1.551 g, 6.14 mmol), and 2-(2-(2-((tetrahydro-2*H*-pyran-2-yl)oxy)ethoxy)ethoxy)ethyl 4-methylbenzenesulfonate (2.643 g, 6.80 mmol) in THF (15 mL), potassium *tert*-butoxide (1.041 g, 9.28 mmol) was slowly added at 0 °C. The mixture was stirred at 25 °C for 11 h. After slowly adding water to the solution, the mixture was extracted with chloroform. The organic layer was washed with brine, dried over anhydrous $MgSO_4$, filtered, and evaporated under reduced pressure. To the residue dissolved in ethanol (30 mL) was added 5% hydrochloric acid (12 mL) and the solution was stirred at 25 °C for 3 h. The mixture was extracted with ethyl acetate. The organic layer was washed with brine and dried over anhydrous $MgSO_4$. After filtration and evaporation of the solvent, the crude product was purified by silica gel column chromatography (eluent: hexane/ethyl acetate = 1 : 1 (v/v)) to give the product (0.930 g, 39% yield). ^{1}H NMR (400 MHz, $CDCl_3$): δ = 3.74–3.60 (m, 12H), 3.22–3.13 (m, 1H), 2.69 (brs, 1H), 2.09–2.01 (m, 2H), 1.78–1.65 (m, 6H), 1.33–0.77 (m, 22H). ^{13}C NMR (100 MHz, $CDCl_3$): δ = 79.1, 72.5, 70.9, 70.6, 70.3, 67.2, 61.7, 42.9, 42.6, 37.8, 37.4, 33.6, 32.4, 32.2, 30.2, 28.2, 26.6, 22.7, 14.1. MS (MALDI-TOF): calcd. (m/z) for $[M + Na]^+$, 407.31; found, 407.01.

Synthesis of compound 2. A mixture of 2-(2-(2-((*trans*,*trans*-4′-pentyl-[1,1′-bi(cyclohexan)]-4-yl)oxy)ethoxy)ethoxy)ethan-1-ol (0.930 g, 2.42 mmol) and KF/Al_2O_3 (0.563 g) in diethyl carbonate (35 mL) was refluxed for 10 h. The reaction mixture was diluted with CH_2Cl_2 and filtered to remove KF/Al_2O_3. After evaporation of the solvent, the crude product was purified by silica gel column chromatography (eluent: hexane/ethyl acetate = 1 : 1 (v/v)) to give compound **2** (0.829 g, 75% yield). ^{1}H NMR (400 MHz, $CDCl_3$): δ = 4.30–4.26 (m, 2H), 4.20 (q, J = 7.2 Hz, 2H), 3.75–3.71 (m, 2H), 3.69–3.60 (m, 8H), 3.21–3.12 (m, 1H), 2.09–2.01 (m, 2H), 1.78–1.65 (m, 6H), 1.34–0.77 (m, 25H). ^{13}C NMR (100 MHz, $CDCl_3$): δ = 155.1, 79.0, 71.0, 70.6, 68.9, 67.2, 66.8, 64.0, 42.9, 42.6, 37.8, 37.4, 33.6, 32.5, 32.2, 30.2, 28.2, 26.6, 22.7, 14.2, 14.1. MS (MALDI-TOF): calcd. (m/z) for $[M + Na]^+$, 479.34; found, 479.18. Elemental analysis: calcd. (%) for $C_{26}H_{48}O_6$: C 68.38, H 10.60; found: C 68.77, H 10.98.

Synthesis of 4-((*trans*,*trans*-4′-pentyl-[1,1′-bi(cyclohexan)]-4-yl)oxy)butan-1-ol. To a stirred mixture of 18-crown-6 (0.902 g, 3.41 mmol), *trans*,*trans*-4′-pentyl-[1,1′-bi(cyclohexan)]-4-ol (0.886 g, 3.51 mmol), and 2-(4-bromobutoxy)tetrahydro-2*H*-pyran (0.918 g, 3.87 mmol) in THF (5 mL), potassium *tert*-butoxide (0.590 g, 5.26 mmol) was slowly added at 0 °C. The mixture was stirred at 25 °C for 15 h. After slowly adding water to the solution, the mixture was extracted with hexane. The organic layer was washed with brine, dried over anhydrous $MgSO_4$, filtered, and evaporated under reduced pressure. To the residue dissolved in ethanol (20 mL) was added 5% hydrochloric acid (2 mL) and the solution was stirred at 25 °C for 5 h. The mixture was extracted with CH_2Cl_2. The organic layer was washed with brine and dried over anhydrous $MgSO_4$. After filtration and evaporation of the solvent, the crude product was purified by silica gel column chromatography (eluent: hexane/ethyl acetate = 80 : 20 (v/v)) to give the product (0.157 g, 14% yield). ^{1}H NMR (400 MHz, $CDCl_3$): δ = 3.63 (t, J = 5.2 Hz, 2H), 3.50 (t, J = 5.6 Hz, 2H), 3.17 (m, 1H), 2.94 (brs, 1H), 2.09–2.01 (m, 2H), 1.80–1.61 (m, 10H), 1.35–0.76 (m, 22H). ^{13}C NMR (100 MHz, $CDCl_3$): δ = 78.8, 67.9, 62.7, 42.9, 42.5, 37.8, 37.4, 33.6, 32.4, 32.2, 30.7, 30.2, 28.1, 27.6, 26.6, 22.7, 14.1. MS (MALDI-TOF): calcd. (m/z) for $[M + Na]^+$, 347.29; found, 346.79.

Synthesis of compound 3. A mixture of 4-((*trans*,*trans*-4′-pentyl-[1,1′-bi(cyclohexan)]-4-yl)oxy)butan-1-ol (0.203 g, 0.63 mmol) and KF/Al_2O_3 (0.118 g) in diethyl carbonate (10 mL) was refluxed for 12 h. The reaction mixture was diluted with CH_2Cl_2 and filtered to remove KF/Al_2O_3. After evaporation of the solvent, the crude product was purified by silica gel column chromatography (eluent: hexane/ethyl acetate = 95 : 5 (v/v)) to give compound **3** (0.211 g, 88% yield). ^{1}H NMR (400 MHz, $CDCl_3$): δ = 4.19 (q, J = 6.8 Hz, 2H), 4.15 (t, J = 6.8 Hz, 2H), 3.47 (t, J = 6.4 Hz, 2H), 3.11 (m, 1H), 2.06–1.99 (m, 2H), 1.79–1.59 (m, 10H), 1.33–0.77 (m, 25H). ^{13}C NMR (100 MHz, $CDCl_3$): δ = 155.2, 78.6, 67.7, 67.2, 63.8, 42.9, 42.6, 37.8, 37.4, 33.6, 32.6, 32.2, 30.2, 28.2, 26.6, 26.4, 25.7, 22.7, 14.3, 14.1. MS (MALDI-TOF): calcd. (m/z) for $[M + Na]^+$, 419.31; found, 418.79. Elemental analysis: calcd. (%) for $C_{24}H_{44}O_4$: C 72.68, H 11.18; found: C 72.74, H 11.18.

Preparation of the mixtures of the LC molecules and LiTFSI

THF solutions containing requisite amounts of the LC molecules and LiTFSI were prepared. The LC mixtures were obtained by slow evaporation of the solvent at 80 °C followed by drying under reduced pressure at 80 °C.

Measurements of ionic conductivities

Ionic conductivities were measured by an alternating current impedance method with a Solartron 1260 impedance/gain-phase analyzer (frequency range: 10 Hz–1 MHz, applied voltage: 0.1 V) equipped with a Linkam 10013L hot stage. The heating rates were fixed at 2 °C min^{-1}. The ionic conductivities were calculated as the product of $1/R$ (Ω^{-1}) and cell constants (cm^{-1}) for the comb-shaped gold electrodes. They were calibrated with a KCl standard solution (HI7033L, 84 μS cm^{-1}) obtained from Hanna Instruments.

Molecular dynamics simulations

All-atom MD simulations of compounds **1** and **2** were performed using the MD program GROMACS 2016.3 and the

models and methodologies followed our previous study.[62] Generalized Amber force field[91] parameters were used for calculating the intra- and intermolecular interactions. The partial atomic charges of the simulated molecule were calculated using the restrained electrostatic potential (RESP)[92] methodology, based on quantum chemical calculations using the B3LYP/6-31G(d) basis set by means of the GAUSSIAN 16 program.[93]

In this study, the pre-equilibration run of single periodic layer in the MD simulation box was initially performed for 5 ns after the steepest energy minimization. For three layers obtained by stacking the single layer structure after the previous MD run, the pre-equilibration run of 5 ns and equilibration run of 500 ns were performed sequentially.

Each layer was composed of 800 molecules and total number of molecules of three layers were 2400.

In the initial structure, a pair of antiparallel molecules was placed on a square grid point in the xy plane. The area per molecule was set to 0.220 nm^2 for both compounds **1** and **2**.

All MD simulations were performed under periodic boundary conditions with constant temperature and pressure. For the pre-equilibration run, the temperature and pressure of the system were kept constant by using the Berendsen thermostat and barostat[94] with relaxation times of 0.2 and 2.0 ps, respectively. The Nosé–Hoover thermostat[95] and the Parrinello–Rahman barostat[96] with relaxation times of 0.2 and 5.0 ps, respectively, were used for the equilibration run. The temperature of both the pre-equilibration and equilibration runs was set to 303 K.

The time step was set to 2 fs since all the bonds connected to hydrogen atoms were constrained with the LINCS algorithm.[97] The smooth particle-mesh Ewald (PME) method[98] was employed to treat the long-range electrostatic interactions with a grid spacing of 0.30 nm. The real space cutoff for both the Coulomb and van der Waals interactions was 1.4 nm.

The time dependencies of the lattice parameter c of the MD simulation box for both compounds **1** and **2** were analyzed as shown in Fig. S20 and S21.† These results indicate that both systems reached at the equilibrium state at 500 ns.

To investigate the orientational order of the system quantitatively, the orientational order parameter was analyzed. The order parameter S was determined as the largest positive eigenvalue of tensor order parameter P obtained from the following equation:

$$P_{\alpha\beta} = \frac{1}{N}\sum_{i=1}^{N}\frac{3}{2}n_{i\alpha}n_{i\beta} - \frac{1}{2}\delta_{\alpha\beta}$$

where n_i is normalized vector of the long axis of the specific group of the molecule, N is the total number of the molecules, and α, β is x, y, z. The orientational order parameters of the rigid core (S_c) and the oligooxyethylene spacer (S_o) were calculated for the long axis vector connecting end atoms of each part as shown in Fig. S22 and S23.†

Data availability

The data supporting this article have been included as part of the ESI.†

Author contributions

T. K. designed the project. T. K., J. U., and G. W. wrote the paper. J. U., S. T., and S. I. performed the experiments and data analysis. S. S. and G. W. conducted the MD simulations. All authors read and commented on the manuscript.

Conflicts of interest

There are no conflicts to declare.

Acknowledgements

This work was supported by JSPS KAKENHI Grant Numbers JP19H05715 and JP19H05718 (Grant-in-Aid for Scientific Research on Innovative Areas of Aquatic Functional Materials).

Notes and references

1 J. Uchida, B. Soberats, M. Gupta and T. Kato, *Adv. Mater.*, 2022, **34**, 2109063.
2 T. Kato, J. Uchida, T. Ichikawa and T. Sakamoto, *Angew. Chem., Int. Ed.*, 2018, **57**, 4355–4371.
3 H. K. Bisoyi and Q. Li, *Chem. Rev.*, 2022, **122**, 4887–4926.
4 T. Kato, M. Gupta, D. Yamaguchi, K. P. Gan and M. Nakayama, *Bull. Chem. Soc. Jpn.*, 2021, **94**, 357–376.
5 S. J. D. Lugger, S. J. A. Houben, Y. Foelen, M. G. Debije, A. P. H. J. Schenning and D. J. Mulder, *Chem. Rev.*, 2022, **122**, 4946–4975.
6 T. Kato, *Science*, 2002, **295**, 2414–2418.
7 T. J. White and D. J. Broer, *Nat. Mater.*, 2015, **14**, 1087–1098.
8 C. Tschierske, *Angew. Chem., Int. Ed.*, 2013, **52**, 8828–8878.
9 N. Kapernaum, A. Lange, M. Ebert, M. A. Grunwald, C. Haege, S. Marino, A. Zens, A. Taubert, F. Giesselmann and S. Laschat, *ChemPlusChem*, 2022, **87**, e20210039.
10 D. L. Gin, X. Lu, P. R. Nemade, C. S. Pecinovsky, Y. Xu and M. Zhou, *Adv. Funct. Mater.*, 2006, **16**, 865–878.
11 T. Kato, N. Mizoshita and K. Kishimoto, *Angew. Chem., Int. Ed.*, 2006, **45**, 38–68.
12 K. Nayani, Y. Yang, H. Yu, P. Jani, M. Mavrikakis and N. Abbott, *Liq. Cryst. Today*, 2020, **29**, 24–35.
13 T. Kato, J. Uchida, Y. Ishii and G. Watanabe, *Adv. Sci.*, 2024, **11**, 2306529.
14 T. Kato, M. Yoshio, T. Ichikawa, B. Soberats, H. Ohno and M. Funahashi, *Nat. Rev. Mater.*, 2017, **2**, 17001.
15 T. Kato, *Angew. Chem., Int. Ed.*, 2010, **49**, 7847–7848.
16 T. Ichikawa, T. Kato and H. Ohno, *Chem. Commun.*, 2019, **55**, 8205–8214.
17 T. Ichikawa, *Polym. J.*, 2017, **49**, 413–421.
18 Y. Zheng, J. Lui, G. Ungar and P. V. Wright, *Chem. Rec.*, 2004, **4**, 176–191.

19 K. Goossens, K. Lava, C. W. Bielawski and K. Binnemans, *Chem. Rev.*, 2016, **116**, 4643–4807.
20 J. Kalhoff, G. G. Eshetu, D. Bresser and S. Passerini, *ChemSusChem*, 2015, **8**, 2154–2175.
21 Y. Nagao, *ChemElectroChem*, 2024, **11**, e202300846.
22 D. Kuo, B. Soberats, K. R. S. Kumar, M. Yoshio, T. Ichikawa, H. Ohno, X. Zeng, G. Ungar and T. Kato, *Mol. Syst. Des. Eng.*, 2019, **4**, 342–347.
23 M. Kumar and S. Kumar, *Polym. J.*, 2017, **49**, 85–111.
24 M. Funahashi, *J. Mater. Chem. C*, 2014, **2**, 7451–7459.
25 W. Pisula, M. Zorn, J. Y. Chang, K. Müllen and R. Zentel, *Macromol. Rapid Commun.*, 2009, **30**, 1179–1202.
26 Y. Shimizu, K. Oikawa, K. Nakayama and D. Guillon, *J. Mater. Chem.*, 2007, **17**, 4223–4229.
27 D. L. Gin and R. D. Noble, *Science*, 2011, **332**, 674–676.
28 M. Henmi, K. Nakatsuji, T. Ichikawa, H. Tomioka, T. Sakamoto, M. Yoshio and T. Kato, *Adv. Mater.*, 2012, **24**, 2238–2241.
29 J. R. Werber, C. O. Osuji and M. Elimelech, *Nat. Rev. Mater.*, 2016, **1**, 16018.
30 D. Kuo, M. Liu, K. R. S. Kumar, K. Hamaguchi, K. P. Gan, T. Sakamoto, T. Ogawa, R. Kato, N. Miyamoto, H. Nada, M. Kimura, M. Henmi, H. Katayama and T. Kato, *Small*, 2020, **16**, 2001721.
31 J. Kloos, N. Joosten, A. Schenning and K. Nijmeijer, *J. Membr. Sci.*, 2021, **620**, 118849.
32 T. Sakamoto, K. Asakura, N. Kang, R. Kato, M. Liu, T. Hayashi, H. Katayama and T. Kato, *J. Mater. Chem. A*, 2023, **11**, 22178–22186.
33 S. Takegawa, K. Hamaguchi, E. Hosono, S. Sato, G. Watanabe, J. Uchida and T. Kato, *Nanoscale*, 2024, **16**, 21118–21127.
34 J. Sakuda, E. Hosono, M. Yoshio, T. Ichikawa, T. Matsumoto, H. Ohno, H. Zhou and T. Kato, *Adv. Funct. Mater.*, 2015, **25**, 1206–1212.
35 A. Kuwabara, M. Enomoto, E. Hosono, K. Hamaguchi, T. Onuma, S. Kajiyama and T. Kato, *Chem. Sci.*, 2020, **11**, 10631–10637.
36 T. Onuma, E. Hosono, M. Takenouchi, J. Sakuda, S. Kajiyama, M. Yoshio and T. Kato, *ACS Omega*, 2018, **3**, 159–166.
37 P.-L. Champagne, D. Ester, A. Bhattacharya, K. Hofstetter, C. Zellman, S. Bag, H. Yu, S. Trudel, V. K. Michaelis, V. E. Williams, V. Thangadurai and C.-C. Ling, *J. Mater. Chem. A*, 2019, **7**, 12201–12213.
38 R. L. Kerr, J. P. Edwards, S. C. Jones, B. J. Elliott and D. L. Gin, *Polym. J.*, 2016, **48**, 635–643.
39 S. Wang, A. Wang, X. Liu, H. Xu, J. Chen and L. Zhang, *Electrochim. Acta*, 2018, **259**, 213–224.
40 D. Gopalakrishnan, S. Alkatie, A. Cannon, S. Rajendran, N. K. Thangavel, N. Bhagirath, E. M. Ryan and L. M. R. Arava, *Sustainable Energy Fuels*, 2021, **5**, 1488–1497.
41 S. Wang, Q. Zeng, A. Wang, X. Liu, J. Chen, Z. Wang and L. Zhang, *J. Mater. Chem. A*, 2019, **7**, 1069–1075.
42 B. Soberats, M. Yoshio, T. Ichikawa, H. Ohno and T. Kato, *J. Mater. Chem. A*, 2015, **3**, 11232–11238.
43 H. Shimura, M. Yoshio, A. Hamasaki, T. Mukai, H. Ohno and T. Kato, *Adv. Mater.*, 2009, **21**, 1591–1594.
44 V. Percec, G. Johansson, J. Heck, G. Ungar and S. V. Batty, *J. Chem. Soc., Perkin Trans. 1*, 1993, 1411–1420.
45 M. Yoshio, T. Mukai, H. Ohno and T. Kato, *J. Am. Chem. Soc.*, 2004, **126**, 994–995.
46 T. H. Do, H.-J. Kim, M. L. Nguyen and B.-K. Cho, *Crystals*, 2020, **10**, 193.
47 T. Ohtake, K. Ito, N. Nishina, H. Kihara, H. Ohno and T. Kato, *Polym. J.*, 1999, **31**, 1155–1158.
48 G. S. McHattie, C. T. Imrie and M. D. Ingram, *Electrochim. Acta*, 1998, **43**, 1151–1154.
49 C. T. Imrie and M. D. Ingram, *Mol. Cryst. Liq. Cryst.*, 2000, **347**, 199–210.
50 K. Kishimoto, M. Yoshio, T. Mukai, M. Yoshizawa, H. Ohno and T. Kato, *J. Am. Chem. Soc.*, 2003, **125**, 3196–3197.
51 Y. Iinuma, K. Kishimoto, Y. Sagara, M. Yoshio, T. Mukai, I. Kobayashi, H. Ohno and T. Kato, *Macromolecules*, 2007, **40**, 4874–4878.
52 Y. Mizumura, D. Högberg, K. Arai, J. Sakuda, B. Soberats, M. Yoshio and T. Kato, *Bull. Chem. Soc. Jpn.*, 2019, **92**, 1226–1233.
53 B. X. Dong, Z. Liu, M. Misra, J. Strzalka, J. Niklas, O. G. Poluektov, F. A. Escobedo, C. K. Ober, P. F. Nealey and S. N. Patel, *ACS Nano*, 2019, **13**, 7665–7675.
54 Z. Liu, B. X. Dong, M. Misra, Y. Sun, J. Strzalka, S. N. Patel, F. A. Escobedo, P. F. Nealey and C. K. Ober, *Adv. Funct. Mater.*, 2019, **29**, 1805220.
55 T. Onuma, M. Yoshio, M. Obi, K. Kashiwagi, S. Tahara and T. Kato, *Polym. J.*, 2018, **50**, 889–898.
56 T. Ohtake, K. Kanie, M. Yoshizawa, T. Mukai, K. Ito-Akita, H. Ohno and T. Kato, *Mol. Cryst. Liq. Cryst.*, 2001, **364**, 589–596.
57 K. Hoshino, K. Kanie, T. Ohtake, T. Mukai, M. Yoshizawa, S. Ujiie, H. Ohno and T. Kato, *Macromol. Chem. Phys.*, 2002, **203**, 1547–1555.
58 A. Eisele, K. Kyriakos, R. Bhandary, M. Schönhoff, C. M. Papadakis and B. Rieger, *J. Mater. Chem. A*, 2015, **3**, 2942–2953.
59 J. Sakuda, M. Yoshio, T. Ichikawa, H. Ohno and T. Kato, *New J. Chem.*, 2015, **39**, 4471–4477.
60 R. Rondla, J. C. Y. Lin, C. T. Yang and I. J. B. Lin, *Langmuir*, 2013, **29**, 11779–11785.
61 D. Bresser, M. Leclere, L. Bernard, P. Rannou, H. Mendili-Jakani, G.-T. Kim, T. Zinkevich, S. Indris, G. Gebel, S. Lyonnard and L. Picard, *ChemSusChem*, 2021, **14**, 655–661.
62 K. Hamaguchi, H. Lu, S. Okamura, S. Kajiyama, J. Uchida, S. Sato, G. Watanabe, Y. Ishii, H. Washizu, G. Ungar and T. Kato, *ChemPhysChem*, 2023, **24**, e202200927.
63 B.-K. Cho, A. Jain, S. M. Gruner and U. Wiesner, *Science*, 2004, **305**, 1598–1601.
64 T. Ichikawa, M. Yoshio, A. Hamasaki, S. Taguchi, F. Liu, X. Zeng, G. Ungar, H. Ohno and T. Kato, *J. Am. Chem. Soc.*, 2012, **134**, 2634–2643.
65 R. L. Kerr, S. A. Miller, R. K. Shoemaker, B. J. Elliott and D. L. Gin, *J. Am. Chem. Soc.*, 2009, **131**, 15972–15973.
66 T. Ichikawa, M. Yoshio, A. Hamasaki, J. Kagimoto, H. Ohno and T. Kato, *J. Am. Chem. Soc.*, 2011, **133**, 2163–2169.

67 X. Gao, F. Lu, L. Shi, H. Jia, H. Gao and L. Zheng, *ACS Appl. Mater. Interfaces*, 2013, **5**, 13312–13317.
68 K. Xu, *Chem. Rev.*, 2004, **104**, 4303–4418.
69 M. Wakihara, *Mater. Sci. Eng., R*, 2001, **33**, 109–134.
70 K. Ariga, *Nanoscale*, 2022, **14**, 10610–10629.
71 A. M. Lowe and N. L. Abbott, *Chem. Mater.*, 2012, **24**, 746–758.
72 I. M. Saez and J. W. Goodby, *J. Mater. Chem.*, 2005, **15**, 26–40.
73 R. Deschenaux, B. Donnio and D. Guillon, *New J. Chem.*, 2007, **31**, 1064–1073.
74 M. Lee, B.-K. Cho and W.-C. Zin, *Chem. Rev.*, 2001, **101**, 3869–3892.
75 J. Uchida and T. Kato, *Liq. Cryst.*, 2017, **44**, 1816–1829.
76 Y. Zhu, S. Zeng, B. Li, A. J. McEllin, J. Liao, Z. Fang, C. Xiao, D. W. Bruce, W. Zhu and Y. Wang, *ACS Appl. Mater. Interfaces*, 2022, **14**, 15437–15447.
77 A. Yoshizawa, *Crystals*, 2024, **14**, 681.
78 H. Eimura, A. Niwa, J. Uchida and T. Kato, *Bull. Chem. Soc. Jpn.*, 2021, **94**, 1588–1593.
79 D. Högberg, B. Soberats, R. Yatagai, S. Uchida, M. Yoshio, L. Kloo, H. Segawa and T. Kato, *Chem. Mater.*, 2016, **28**, 6493–6500.
80 S. Ujiie and K. Iimura, *Macromolecules*, 1992, **25**, 3174–3178.
81 S. Ahn, S. Yamakawa and K. Akagi, *J. Mater. Chem. C*, 2015, **3**, 3960–3970.
82 J. Uchida, M. Yoshio and T. Kato, *Chem. Sci.*, 2021, **12**, 6091–6098.
83 Y. Wang, C. P. Cabry, M. Xiao, L. Male, S. J. Cowling, D. W. Bruce, J. Shi, W. Zhu and E. Baranoff, *Chem. – Eur. J.*, 2016, **22**, 1618–1621.
84 J. Uchida, M. Yoshio, S. Sato, H. Yokoyama, M. Fujita and T. Kato, *Angew. Chem., Int. Ed.*, 2017, **56**, 14085–14089.
85 A. Martinez-Felipe, D. Zaton, M. Castillo-Vallés, A. Baldini, J. Pease, N. Leader, N. F. K. Aripin, M. Giacinti-Baschetti and M. B. Ros, *J. Mol. Liq.*, 2023, **390**, 123100.
86 M. Yoshio, T. Mukai, M. Yoshizawa, H. Ohno and T. Kato, *Mol. Cryst. Liq. Cryst.*, 2004, **413**, 99–108.
87 J. Uchida, A. Niwa, M. Hasome, R. Makiura, N. L. Abbott and T. Kato, *ACS Appl. Mater. Interfaces*, 2023, **15**, 36657–36666.
88 L. J. O'Driscoll, D. J. Welsh, S. W. D. Bailey, D. Visontai, H. Frampton, M. R. Bryce and C. J. Lambert, *Chem. – Eur. J.*, 2015, **21**, 3891–3894.
89 W. Li, D. Wu, A. D. Schlüter and A. Zhang, *J. Polym. Sci., Part A: Polym. Chem.*, 2009, **47**, 6630–6640.
90 L. Emert-Sedlak, T. Kodama, E. C. Lerner, W. Dai, C. Foster, B. W. Day, J. S. Lazo and T. E. Smithgall, *ACS Chem. Biol.*, 2009, **4**, 939–947.
91 J. Wang, R. M. Wolf, J. W. Caldwell, P. A. Kollman and D. A. Case, *J. Comput. Chem.*, 2004, **25**, 1157–1174.
92 I. Bayly, P. Cieplak, W. D. Cornell and P. A. Kollman, *J. Phys. Chem.*, 1993, **97**, 10269–10280.
93 M. J. Frisch, G. W. Trucks, H. B. Schlegel, G. E. Scuseria, M. A. Robb, J. R. Cheeseman, G. Scalmani, V. Barone, G. A. Petersson, H. Nakatsuji, X. Li, M. Caricato, A. Marenich, J. Bloino, B. G. Janesko, R. Gomperts, B. Mennucci, H. P. Hratchian, J. V. Ortiz, A. F. Izmaylov, J. L. Sonnenberg, D. Williams-Young, F. Ding, F. Lipparini, F. Egidi, J. Goings, B. Peng, A. Petrone, T. Henderson, D. Ranasinghe, V. G. Zakrzewski, J. Gao, N. Rega, G. Zheng, W. Liang, M. Hada, M. Ehara, K. Toyota, R. Fukuda, J. Hasegawa, M. Ishida, T. Nakajima, Y. Honda, O. Kitao, H. Nakai, T. Vreven, K. Throssell, J. A. Montgomery Jr , J. E. Peralta, F. Ogliaro, M. Bearpark, J. J. Heyd, E. N. Brothers, K. N. Kudin, V. N. Staroverov, T. Keith, R. Kobayashi, J. Normand, K. Raghavachari, A. Rendell, J. C. Burant, S. S. Iyengar, J. Tomasi, M. Cossi, J. M. Millam, M. Klene, C. Adamo, R. Cammi, J. W. Ochterski, R. L. Martin, K. Morokuma, O. Farkas, J. B. Foresman and D. J. Fox, *Gaussian 16, Revision C.01*, Gaussian, Inc., 2016.
94 H. J. C. Berendsen, J. P. M. Postma, W. F. van Gunsteren, A. DiNola and J. R. Haak, *J. Chem. Phys.*, 1984, **81**, 3684–3690.
95 S. Nosé, *Mol. Phys.*, 1984, **52**, 255–268.
96 M. Parrinello and A. Rahman, *J. Appl. Phys.*, 1981, **52**, 7182–7190.
97 B. Hess, H. Bekker, H. J. Berendsen and J. G. Fraaije, *J. Comput. Chem.*, 1997, **18**, 1463–1472.
98 T. Darden, D. York and L. Pedersen, *J. Chem. Phys.*, 1993, **98**, 10089–10092.